

---

# Testing the Reliability of PN Structures Detected by the Wavelet Technique

M.L. Leal Ferreira<sup>1</sup>, C.R. Rabaça<sup>1</sup>, F.C. Cuisinier<sup>1</sup> and D.N. Epitácio Pereira<sup>2</sup>

<sup>1</sup> Observatório do Valongo/UFRJ – Rio de Janeiro (Brazil) [ferreira@ov.ufrj.br](mailto:ferreira@ov.ufrj.br),  
[rabaca@ov.ufrj.br](mailto:rabaca@ov.ufrj.br), [francois@ov.ufrj.br](mailto:francois@ov.ufrj.br)

<sup>2</sup> Observatório Nacional – Rio de Janeiro (Brazil) [dnep@on.br](mailto:dnep@on.br)

**Summary.** One of the advantages of the application of the wavelet technique to planetary nebulae (PNe) is the possibility to extract the noise from the images using thresholds based on the spatial frequencies of the identified structures. The detection of new structures in the nebulae not previously mentioned in the literature has made us wonder about the reliability and the efficiency limit of the technique. Are these detections false, artificially created, or in fact real? This work presents the results of four tests performed on HST images of NGC7009 taken with a range of signal-to-noise ratios, and support the idea that the structures found are real and the technique very reliable.

**Key words:** planetary nebula, wavelet, NGC7009

## 1 The Method

We have used the `OV_WAV` package, developed at the Observatório do Valongo/UFRJ, which implements the “à trous” (with holes) wavelet technique (Shensa 1992), and an adaptation of the multiscale vision model proposed by Bijaoui & Rue (1995). With the application of this technique to an astronomical image, we decompose it on several new images of the same size as the original one, containing only wavelet coefficients plus a residual image. Each one of the new wavelet coefficient images can be identified with a plane in which only structures of a single characteristic scale size can be seen. The algorithm does not employ an orthogonal basis and because of that, it generates redundant information. Redundancy is very important to this problem since we deal with weak signals, but requires the use of some modeling for the reconstruction of the source of the signal. According to the adopted model, a single object<sup>3</sup> derives from a finite set of structures (defined from thresholds established at the different planes) linked hierarchically from smallest to largest size solely on the basis of its position on the image. The plane in which we find the structure with the highest flux in the set defines the object characteristic

---

<sup>3</sup> An object is identified as an emission region of the nebulae or a back/foreground object.

size and all structures up to that scale are used to solve the inverse problem of recovering the actual brightness distribution and the flux of the object. The identified and modeled (reconstructed) objects are then subtracted from the original image. If the residual image still presents some signal associated to the PN, the whole procedure is reapplied to it. The cycle can be repeated as many times as we want and are needed in order to obtain a final residual image without any sources of identifiable signal.

## 2 Data Processing

The NGC7009 images used were taken with the F502N (5007 Å) filter in the WFPC-2 HST camera. Three independent images were used in this work: one with exposure time of 40 sec, and two with 160 sec. A fourth image was generated by adding up the two 160 sec images, resulting in a 320 sec image. They are presented in Fig. 1a (after some processing). Data processing (bad mask correction, cosmic ray subtraction and mosaic) has been done with IRAF. Finally, all images were set to the same orientation in the sky. This last step was performed only after the wavelet modeling.

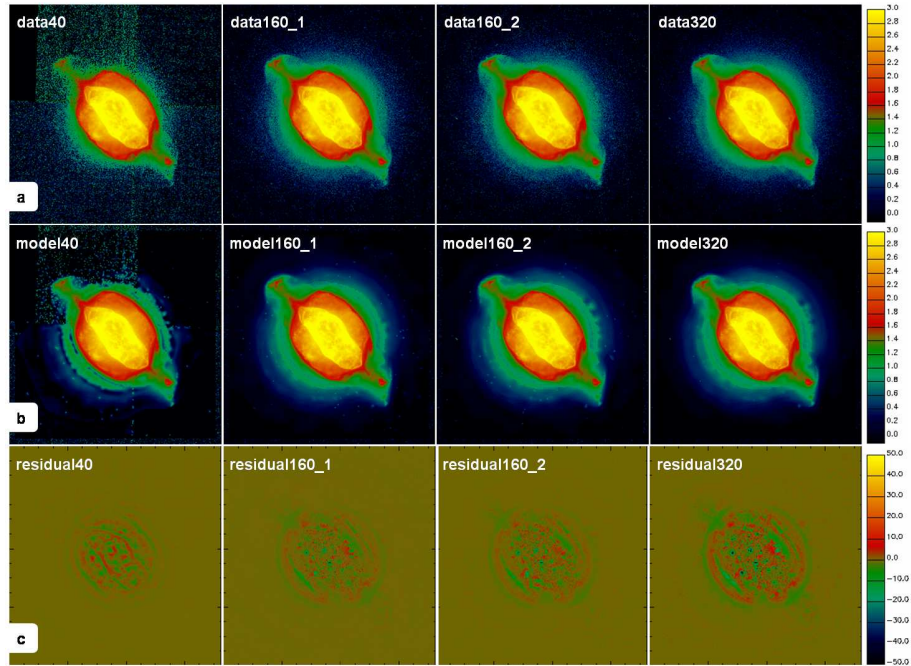


**Fig. 1.** NGC7009 imagery: (a) HST direct images and (b) wavelet models are shown in a logarithmic scale; (c) residuals shown in a linear scale

### 3 Models and Residuals

The wavelet models (Fig. 1b) were obtained using 10 scale sizes, and three modeling cycles. Note that the removal of the noise allows the PN halo to be seen. The final residual images (model – data) (Fig. 1c) have noise levels that are in agreement with the Poisson noise present in the original HST signal; it is possible though that some very low surface brightness structures are still present on them.

## 4 Results

### 4.1 First Test: Comparison between Model Images with Same Exposure Times

The two 160 sec models should not present different structures if the modeling is reliable. In the analysis, we subtracted one model from the other and found no evidence of different morphological structures (Fig. 2a). This difference is very similar to the difference between the original HST images as well (Fig. 2b). Note that the largest values in both differences are equivalent and have the same intensity levels seen in residual160\_1 and residual160\_2, what suggest that the differences are mostly due to noise. Both models also present a very similar number of detected objects (223 and 249 objects for model160\_1 and model160\_2, respectively), confirming the hypothesis a reliable modeling.

### 4.2 Second Test: Comparison between Model Images with Different Exposure Times

The morphological structures identified in the 40 sec and in the 320 sec models should be equivalent and characterize very well the PN. Small differences may occur as consequence of their different signal-to-noise ratios (SNR). Subtracting model320 from eight times model40, we got no evidence of different morphological structures (Fig. 2c). The highest values were located in the central region of the PN; this is expected because the peak intensities and fluctuations are located in this region. The difference between models shows the same levels as the difference between the two HST images (Fig. 2d) and agrees with the levels seen in residual40 and residual320 as well. The different number of identified objects in each model (695 and 211 objects for model40 and model320, respectively) led us to the third test.

### 4.3 Third Test: Determination of the Reliability of the Identified Structures through a Signal-to-Noise Ratio Cutoff

The rejection of the identified objects with lowest SNR should only remove low confidence level objects from the models. Based on that, we have removed from model40 all objects with  $\text{SNR} \leq 3$  and scale sizes of  $2^1$  pixels, with  $\text{SNR} \leq 2$  and scale sizes  $2^2$  pixels, and with  $\text{SNR} \leq 1$  for all larger scale sizes. For model320, we adopted a cutoff at  $\text{SNR} = 1$  for all scale sizes. The number of objects that survived the cutoffs are 340 and 205, respectively, for model40 and model320. In Fig. 3, we

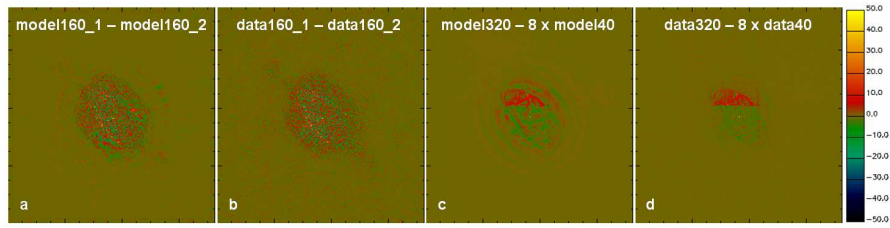


**Fig. 2.** Difference images: (a) between the 160 sec models, b) between the HST 160 sec images, c) between the 320 sec and 40 sec models, and d) between the 320 sec and 40 sec HST images

present the distribution of (x,y) coordinates for the center of (a) all objects identified in both models, and (b) objects that survived the SNR cutoffs only. Note that in model40 many objects located over the PC quadrant were eliminated. These objects should not be real; in fact they are mostly due to noise. On the other hand, in model320 only 6 objects were eliminated. In Fig. 3c we present the image of the PN reconstructed from model40 with the surviving objects only.

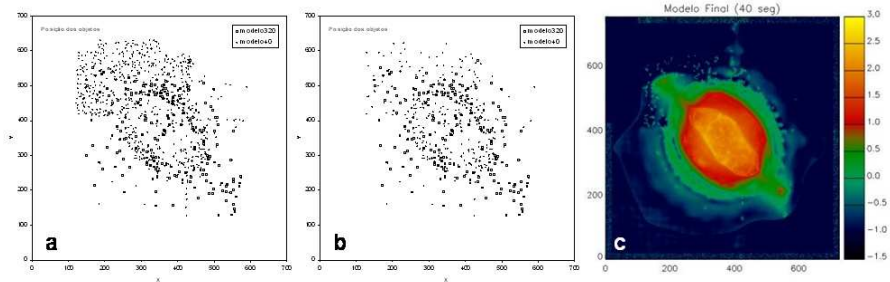


**Fig. 3.** Distributions of object centers for (a) all the objects identified in model40 and model320, and (b) objects that survive the SNR cutoffs only. (c) Image of the PN reconstructed from model40 with the surviving objects only

#### 4.4 Fourth Test: Application of the Wavelet Technique to a Halo Subtracted Image

Since an object is reconstructed from a finite number of wavelet scales, we wanted to test whether the extended halo could be the result of a bad modeling of the inner bright part of the nebula. Therefore, we created a new image from model320 in which the objects associated to the extended halo were completely removed (Fig. 4a). We then added residual320 to this image, in order to insert the original noise. Finally, we applied the wavelet technique to the resulting image. Both the wavelet model (Fig. 4b) and the residual image (Fig. 4c) do not show any indication of an extended structure. Therefore, the technique is not responsible for producing the detected halo.

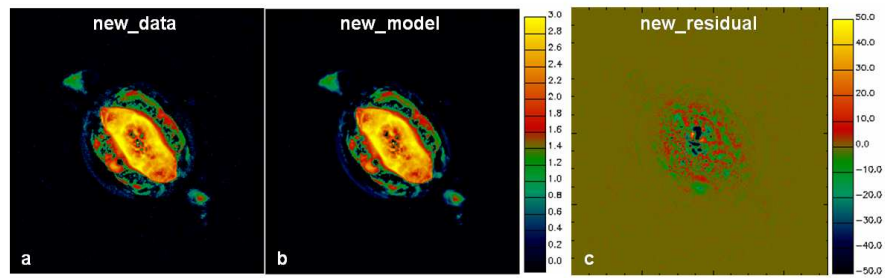


**Fig. 4.** (a) The new data created from the halo subtracted model320 plus residual320, (b) the corresponding wavelet model, and (c) the final residual image

## 5 Conclusions

Denoising and reconstruction of PNe images with the wavelet technique were found to be very reliable. Our tests on HST images of NGC7009 showed that the main structures detected are coherent among the different wavelet models produced, and the residuals between original images and wavelet models reveal no significant structures. We have also confirmed that the technique is not able to create extended artificial halos. Our confidence in the detected objects can be enhanced if we establish a cutoff limit based on the SNR. Low SNR objects in general have small sizes and low fluxes. The SNR cutoff is able to reject spurious objects while keeping the overall structure of the PN unaltered.

## References

1. A. Bijaoui, F. Rue: *Signal Processing* **45**, 345–362 (1995)
2. M.J. Shensa: *IEEE Transactions on Signal Processing* **40**, pp 2464–2482 (1992)